Electronic Supplementary Material (ESI) for Biomaterials Science.

Supplementary Information

Magnetically Controlled Cyclic Microscale Deformation of *in vitro* Cancer Invasion Models

Authors: Daphne O. Asgeirsson[1], Avni Mehta[1], Anna Scheeder[1,2], Fan Li[1], Xiang Wang[1], Michael G. Christiansen[1], Nicolas Hesse[1], Rachel Ward[1], Andrea J. De Micheli[1,3], Ece Su Ildiz[4], Stefano Menghini[1], Nicola Aceto[4], Simone Schuerle[1]

Affiliations

[1] Responsive Biomedical Systems Laboratory, Department of Health Science and Technology, ETH Zurich, 8093 Zurich, Switzerland

[2]Department of Chemical Engineering and Biotechnology, University of Cambridge, Cambridge CB3 0AS, U.K.

[3] Department of Oncology, Children's Research Center, University Children's Hospital Zurich, Zurich 8032, Switzerland

[4]Department of Biology, Institute of Molecular Health Sciences, ETH Zurich, 8093 Zurich, Switzerland

Supplementary Text 1: Fabrication of Magnetic Iron µRods

Magnetic iron µRods were fabricated using template restricted electrodeposition. The method to prepare plating templates via photolithography was adapted from work by B. Özkale.[1]

Preparation of Plating Templates

For the preparation of plating templates, 4-inch Si-wafers were coated with a conductive layer of 25 nm titanium and 125 nm gold using electron-beam evaporation (MEB550S, Plassys). The wafer was pre-baked at 200 °C for 10 minutes to remove any hydration layer on the surface and spin coated with a first layer of photoresist (10XT, 520 cp, MicroChemicals) at 500 rpm for 10 seconds followed by 2'400 rpm for 60 seconds. The wafer was soft baked at 110 °C for 80 seconds and left to rehydrate for 10 minutes. Next, a second layer of photoresist was applied using previously listed spin parameters and soft baked at 110°C for 160 seconds. For rehydration, the coated Si-wafer was stored at ambient conditions for 45 minutes prior to exposure. Exposure of the photoresist was performed using a mask aligner (EVG 620 NT, EVG) with a chrome mask designed for arrays of pores with a diameter of 5 µm in a distance of 15 µm (Jena masks, Germany) at a dose of 400 kJ/cm^2.

Post exposure, samples were developed using AZ 400 K developer (MicroChemicals) at a dilution of 1:3 for 17 minutes under gentle agitation and exchange of developer after 10 minutes of incubation. Samples were rinsed in excess with deionized water and dried with pressured air. Si-wafers were diced into chips of 2*3 cm^2 for plating experiments using a diamond scribe.

Plating of µRods

Plating of iron µRods was performed using photoresist-based templates which were prepared as specified in the previous section. The plating templates were subjected to oxygen-plasma treatment for 30 seconds prior to electroplating experiments to enhance surface wetting.

The electrodeposition methodology was adapted from Alcantara et al.[2] The electrolyte solution was prepared with amounts as specified in **Supplementary Table 1**. Deionized water was added to reach a final volume of 200 mL and the solution was stirred at 250 rpm with a magnetic stirrer at 50°C to obtain a green transparent electrolyte solution. Concentrated sulfuric acid (Sigma-Aldrich) was added dropwise to adjust the solution to pH 2 and the stirring frequency was reduced to 50 rpm for the plating experiments. Plating templates were connected to the working electrode and immersed in the electrolyte solution together with a 5*5 cm platinum sheet counter electrode and Ag/AgCl reference electrode. A potential of -0.95 V against the reference electrode was applied for 40 minutes to obtain iron µRods with an approximate length of 25 µm. After plating, samples were removed from the electrolyte solution, rinsed with deionized water, and dried with pressured air.

The photoresist template was removed by thorough washing with acetone and isopropanol, gently dried with pressured air. A protective layer of silicon oxide (SiOx) with a thickness of approximately 60 nm was applied via plasma enhanced chemical vapor deposition (PECVD 80+, Oxford Instruments). The SiOx-layer provided a bioinert

shell around the µRods to prevent corrosion and the leakage of iron or iron oxides into the surrounding aqueous environment.

SEM Imaging of µRods in Col I

For SEM imaging of Col I hydrogels enriched with iron µRods, Col I hydrogels were prepared as specified above and supplemented with 5 µL of surface-functionalized iron µRods. Hydrogels were pipetted on round pieces of filter paper and left to polymerize at 37°C, 5% CO_2 in a standard cell culture incubator for 45 minutes. Samples were fixed for 1 hour in glutaraldehyde, thoroughly washed with deionized water and dehydrated by means of serial incubation with increasing concentrations of ethanol. Samples were subjected to critical point drying and sputtered with Pd/Au prior to imaging.

Surface Functionalization of Iron µRods

A surface functionalization of the SiOx-coated iron µRods was performed to allow for stable attachment of the iron µRods to the surface of Col I hydrogel networks via amidation. To stably link the surface of SiOx-coated iron µRods to the fibrous network of Col I hydrogels, surface of the coated µRods was silanized to obtain free amine groups (NH_2) on the particle surface. Next, an NHS-PEG-NHS linker was grafted onto the NH_2 groups. The functionalization strategy is depicted in **Supplementary Figure S1** and is described in the following paragraphs.

Amine Functionalization of SiOx-Coated µRods

The silanization process of the SiOx-coated iron µRods was adapted from Kim et al.[3] Clean and dry SiOx-coated sample chips were placed in 50 mL Falcon tubes and covered with a solution of 2% 3-Aminopropyltriethoxysilane (APTES, 99%, Acros) that had been prepared with anhydrous toluene (extra dry, Fisher Scientific). Samples were incubated for 4 hours at room temperature under gentle agitation, rinsed two times for 10 minutes with toluene and dried with nitrogen. Until further use, samples were stored in filtered deionized water at 4°C.

Grafting of NHS-PEG-NHS on the Surface of Amine-Functionalized µRods

For stable attachment of iron µRods to free amines of Col I networks, NHS-groups were grafted on amine groups of silanized µRods according to a previously published method.[4] Amine-functionalized µRod chips were incubated with a solution 5 mg/mL NHS-PEG-NHS (4-arm PEG, 5k, Creative PEG Works) in TEA buffer (0.1 M, pH 6) and incubated at RT under gentle agitation for 30 minutes. Samples were washed twice in TEA buffer (0.1 M, pH 6) and sonicated for a few seconds to release functionalized µRods from the plating substrate.

Experimental Verification of µRod Surface Functionalization

Silanized and non-silanized µRods were incubated with 5(6)-TAMRA *N*-succinimidyl ester (C0027, Chemodex, hereafter referred to as NHS-TAMRA) diluted at a concentration of 5 mg/mL in 0.1 M TEA buffer (pH 6) for 30 minutes under gentle agitation at room temperature and thoroughly washed twice with 0.1 M TEA buffer (pH 6). Samples were briefly sonicated to disperse the µRods.

Drops of µRod suspension were pipetted on a microscopy slide and imaged via fluorescence confocal microscopy (Nikon Eclipse) in the TEXAS Red channel (580 nm) (**Supplementary Figure S2)**, confirming the attachment of the NHS-TAMRA dye to the µRod surface via amidation. The control sample of non-silanized, SiOx-coated µRods, which had been incubated with the same dye, did not exhibit a signal, confirming that the fluorescent labeling of the silanized sample was not caused by unspecific binding of the dye to the µRod. Similarly, the successful grafting of NHS-groups onto the silanized µRod surface was experimentally confirmed.

Following the functionalization of µRods with NHS-PEG-NHS groups as described before, µRods were incubated with an Amine-Cy3 dye (Cyanine3-amine, Lumiprobe) that was diluted in 0.1 M TEA buffer (pH 6) at a concentration of 5 mg/mL for 30 minutes under gentle agitation at room temperature. As a control, NHS-PEG-NHS functionalized µRods were simultaneously incubated with a 50 M Tris-acetate-EDTA (TAE) buffer to quench any reactive NHS sites with an excess of amines present in the buffer. Next, both the quenched control and the Amine-Cy3 labelled µRods were washed with 0.1 M TEA buffer (pH 6). Then, to test for unspecific binding of the dye, the Amine-Cy3-labelled µRods were incubated with the previously described quenching solution while the NHS-quenched µRods were incubated with the previously specified Amine-Cy3 labeling solution. In both cases incubation lasted 30 minutes. Subsequently, samples were rinsed twice with 0.1 M TEA buffer (pH 6) and sonicated to disperse the µRods. Drops of the µRod suspensions were pipetted onto microscopy slides and imaged via confocal fluorescence microscopy to test for fluorescence signal. A strong signal of Amine-Cy3 labelling was detected for the NHS-PEG-NHS-functionalized µRods while the quenched samples do not exhibit a clear fluorescence signal (**Supplementary Figure S2c**), indicating that the quenching procedure blocked all available NHS-groups prior to the fluorescent labeling and that the unquenched samples exhibited reactive NHS-groups that were well reacted with the amines of the Amine-Cy3 dye.

Magnetic Characterization of Iron µRods

SiOx-coated µRods were magnetically characterized via vibrating sample magnetometry (VSM). To prepare the sample, Polydimethylsiloxane (PDMS) polymer (SYLGARD™ 184 Silicone Elastomer, Dow) was mixed according to manufacturer's instructions and degassed for 1 hour. 1.5 mg of SiOx-coated µRods were dispersed in 100 µL degassed PDMS that was then poured in a mold ring of cured PDMS with 8 mm diameter that had been previously prepared in a plastic dish. The sample was degassed again for 1 hour at room temperature and then cured at 80°C for 3 hours. Using a metal puncher with 8 mm diameter, the PDMS containing magnetic µRods was punched out of the template. A background control sample was prepared accordingly without addition of magnetic µRods.

For VSM measurements (**Supplementary Figure S3**), sample disks were glued to the sample holder (8 mm Pyrex Transverse) using double sided tape. A hysteresis loop was measured using a vibrating sample magnetometer (EZ-VSM, Microsense). The background signal from the sample holder and blank PDMS sample was measured and subtracted from the signal collected for the µRod-containing sample.

Biocompatibility Analysis of Iron µRods

Biocompatibility of functionalized iron µRods was tested via an MTT assay (**Supplementary Figure S4)**. Cells of the invasive cancer cell line MDA-MB-231 GFP cells were cultured as described above and were seeded in 96-well plates at a density of 10^4 cells/well. After one day of culture, 97 µL of the respective cell culture medium were added together with functionalized µRods dispersed in 3 µL of 0.1 M TEA in two different amounts (Low Concentration: 50 µRods per well; High Concentration: 250 µRods per well). Further, for the vehicle control, 97 µL of culture medium were supplemented with 3 µL of 0.1 TEA buffer without µRods and an untreated control was provided with 100 µL of fresh cell culture medium. All samples were prepared in triplicate and analyzed via the MTT assay 1, 2, and 3 days after µRod addition. Cell viability was quantified using the CyQuant MTT Cell Viability Assay (Thermo Fisher Scientific, V13154). After 10 minutes of cell incubation with the reaction mix at 37°C and 5% CO_2, samples were gently agitated and a multimode microplate reader (Spark, Tecan) was used to measure absorbance at 540 nm. The experiment was performed using triplicates.

Supplementary Text 2: Image Processing

Imaging of spheroids embedded in Col I hydrogels was performed with 10x magnification and image stacks were acquired with 8 µm distance and a total of 11 images per stack. During imaging, care was taken to center the equatorial region of the spheroid in the center of the stack, to capture the maximum spread and flanking regions. Imaging of spheroids was performed 1 hour after embedding, and after 18 hours and 42 hours of incubation.

If not indicated differently, acquired images were processed using FIJI. Analysis of spheroid morphology in Col I hydrogels was performed the following way using FIJI: Z-projections of image stacks acquired of green-fluorescent tumor spheroids were generated and saved as .tiff files. All images were subjected to the same adjustment regarding window level, converted to binary files, thresholded and analyzed using the particle analyzer function of FIJI. Parameters extracted from the image data included projected area and centroid point of the primary tumor and its subsequent invading cells, the minimal and maximal Feret diameter, including the x and y axis of the spheroid, depending on the intended analysis. The invasion zone of each spheroid was calculated by measuring the distance (µm) of the top five furthest travelled cells from the rim of the tumor.

Supplementary Text 3: Explanation of Torque Estimation for µRods

The soft ferromagnetic µRods employed in this study consist of metallic iron and are large enough to support multiple magnetic domains. Under the application of an external magnetic field such as the 50 mT field used in actuation experiments, they can be regarded as approximately uniformly magnetized and experience anisotropy dominated by shape effects, with their uniaxial easy axis coinciding with the axis of the cylinder. At low fields, the magnitude of the torque will scale proportionally with the moment of the µRod $\vec{m}$ and the applied field $\vec{B}$, with its upper limit $|\vec{\tau}|_{max}$ given by

$$|\vec{\tau}|_{max} = |\vec{B}||\vec{m}|$$

For the purpose of estimating this value for the μRods used in this work, we can assume an applied field magnitude of 50 mT, a μRod length l of 25 μm, a μRod diameter d of 7 μm, and a saturation magnetization M_s corresponding to that of bulk metallic iron.[5]

$$|\vec{\tau}|_{max} \approx 0.05T \cdot \pi \cdot (3.5 \times 10^{-6}m)^2 \cdot 25 \times 10^{-6}m \cdot 1.71 \times 10^{6} A\,m^{-1} = 8.2 \times 10^{-12} N\,m$$

During cyclic actuation by rotating magnetic fields, this maximum torque would only be reached briefly during the part of the cycle when the moment is perpendicular to the field. It should additionally be noted that the absolute upper bound of available torques that can be supplied with a μRod of this type is set by the energy scale of the magnetic shape anisotropy. In the limit of high applied fields, the moment would be oriented away from its easy axis, but a torque resulting from shape anisotropy would still be experienced. The estimate employed above assumes that the moment is still confined to the easy axis under the applied field, an assumption that can be supported by comparing that torque value to that of the ultimate torque available from shape anisotropy. The magnetostatic energy U of a magnetized cylinder with its moment oriented at angle θ relative to the axis of the cylinder is

$$U(\theta) = \frac{1}{2}\mu_0 {M_s}^2 V\left(\frac{1 - 3\,N_z}{2}\sin^2\theta + N_z\right)$$

The demagnetizing factors for cylinders, $N_x = N_y$ and N_z, expressed as a function of their aspect ratio n, where $n = l/d$ (length over diameter), have been computed numerically and can also be given by approximate analytical functions.[6] The torque τ resulting from this potential energy function is

$$\tau = -\frac{\partial U}{\partial \theta} = -\frac{1}{2}\mu_0 {M_s}^2 V(1 - 3\,N_z)\cos\theta\sin\theta$$

With the dimensions assumed above, the aspect ratio is approximately 3.6, giving an N_z value of approximately 0.11. Thus, for the μRods employed in this work, the absolute maximum applicable torque is estimated to be

$$|\vec{\tau}|_{max,abs} = \frac{1}{4}\mu_0 {M_s}^2 V(1 - 3 \cdot 0.11) \approx 6.0 \times 10^{-10}\,N\,m$$

Because this value is approximately two orders of magnitude higher than the torque estimated using just the applied field and the moment of the μRod, it is clear that the earlier estimate assuming that the moment is largely confined to the easy axis is well motivated for the conditions we employed in this study.

Supplementary Table 1: Composition of the electroplating solution

Reagent	Amount	Supplier
Iron Sulfate Heptahydrate $FeSO_4< 7H_20$	50.5 g	Sigma-Aldrich
Iron(II)chloride tetrahydrate $FeCl_2$ $4H_2O$	8.8 g	Sigma-Aldrich
Ammonium Chloride NH_4Cl	5.4 g	Sigma-Aldrich

The table lists the components for the preparation of an electrolyte solution for the electrodeposition of iron µRods

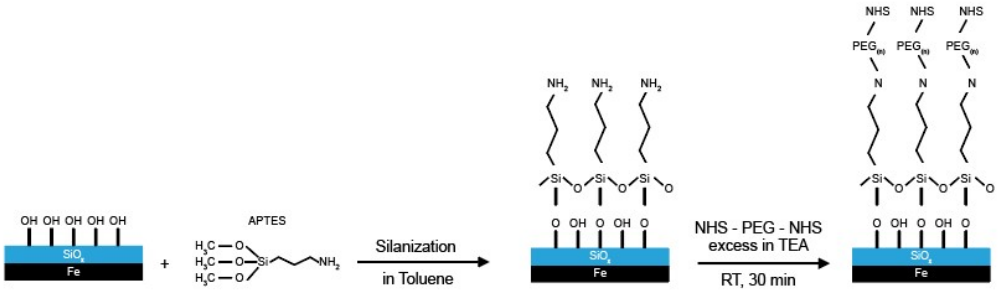

Supplementary Figure S1: Amine functionalization of µRods

The schematic depicts different stages of the surface functionalization strategy of SiOx-coated iron µRods to obtain NHS-groups that can bind to free amines exposed by the Col I network via amidation. The illustrated process is described in the Materials & Methods section.

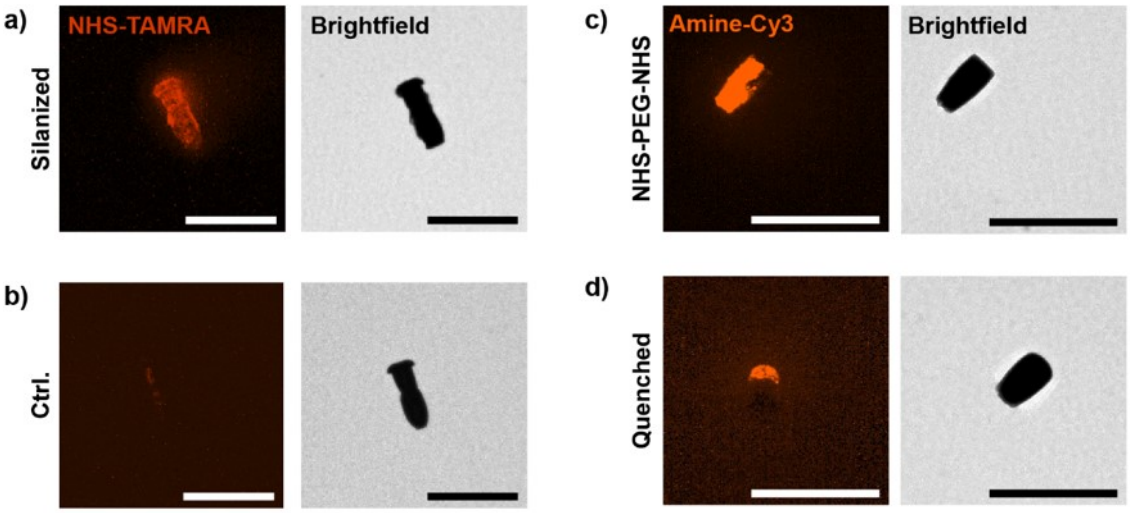

Supplementary Figure S2: Experimental verification of SiOx µRod surface functionalization via fluorescence confocal microscopy a-b) Silanized and untreated µRods were incubated with an NHS-TAMRA ester. **a)** Confocal fluorescence (left) and brightfield image (right) of a silanized µRod that was exposed to a solution of NHS-TAMRA to stain for free amines on the µRods surface. **b)** Confocal fluorescence (left) and brightfield image (right) of a non-silanized µRod that was exposed to the same staining solution as the sample shown in a). **c-d)** An Amine-Cy3 dye was used to test for the presence of reactive NHS-groups on the µRod surface after surface functionalization of the µRods with an NHS-PEG-NHS ester. **c)** Confocal fluorescence (left) and brightfield image (right) of a NHS-PEG-NHS-functionalized µRod labelled with an Amine-Cy3 dye, indicating the presence of active NHS groups. **d)** Confocal fluorescence (left) and brightfield image (right) of a NHS-PEG-NHS-functionalized µRod which had been quenched with a 50 M TAE buffer to block all present NHS groups prior to labeling with an Amine-Cy3 dye. All images are representative examples. All scale bars: 50 µm.

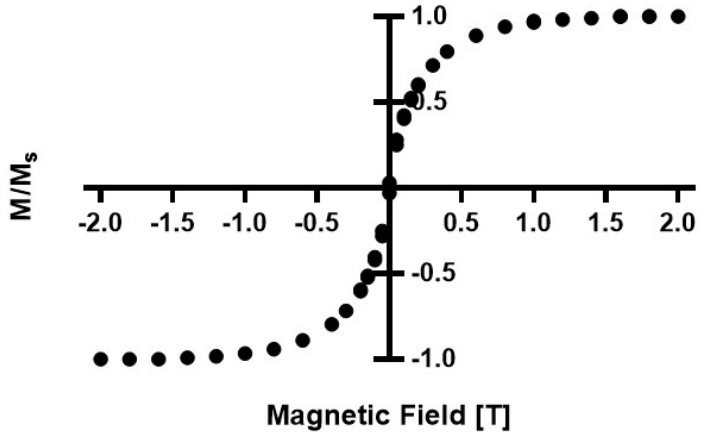

Supplementary Figure S3 Vibrating sample magnetometry (VSM) analysis of iron µRods.

The data from the VSM measurement confirm the ferromagnetic character of the iron µRods.

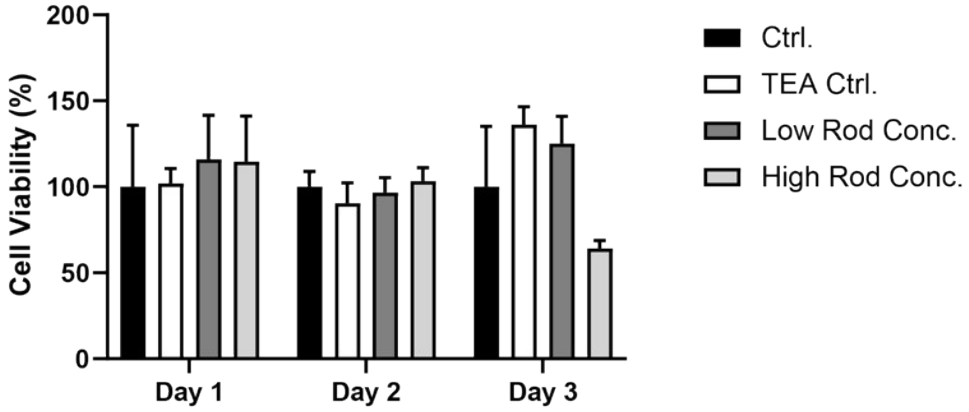

Supplementary Figure S4: Biocompatibility analysis of surface functionalized iron µRods tested via MTT assay Data is shown for MDA MD 231 GFP cells that were cultured in the presence of different µRod concentrations and tested for viability over three days of culture. Ctrl: No treatment; TEA Ctrl: 3 µL of 0.1 M TEA buffer without µRods; Low µRods Conc.: 50 µRods dispersed in 3 µL of TEA buffer per well; High Rod Conc.: 250 µRods dispersed in 3 µL of TEA buffer per well. (n=3) Significance was tested using the Turkey's multiple comparison test and no significant difference was found between the conditions. The results suggest that no significant toxicity could be detected for neither the high nor low µRod concentrations.

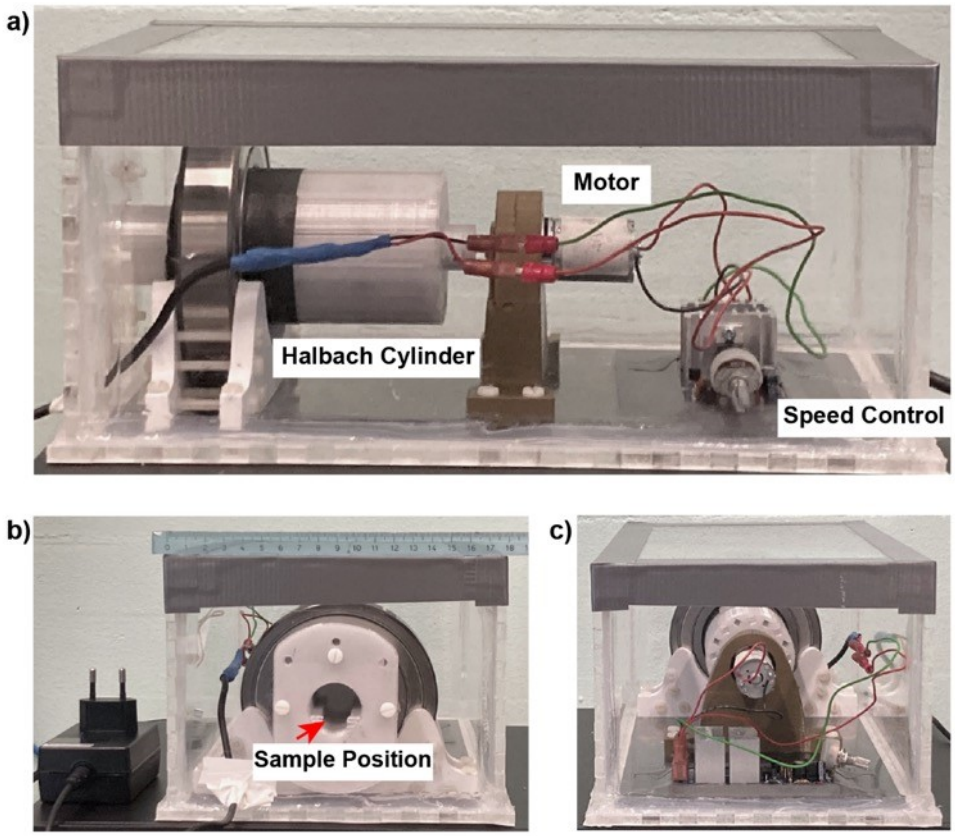

Supplementary Figure S5: Overview of the Halbach-cylinder-based magnetic field generator.
Photographs show the magnetic actuation setup which is encased in a sealed acrylic box. **a)** side view, indicating the position of the Halbach cylinder, the actuating motor and the speed controller. **b)** Front view of the setup, indicating the position where sample slides were introduced to the system for long-term actuation. **c)** Rear view of the setup.

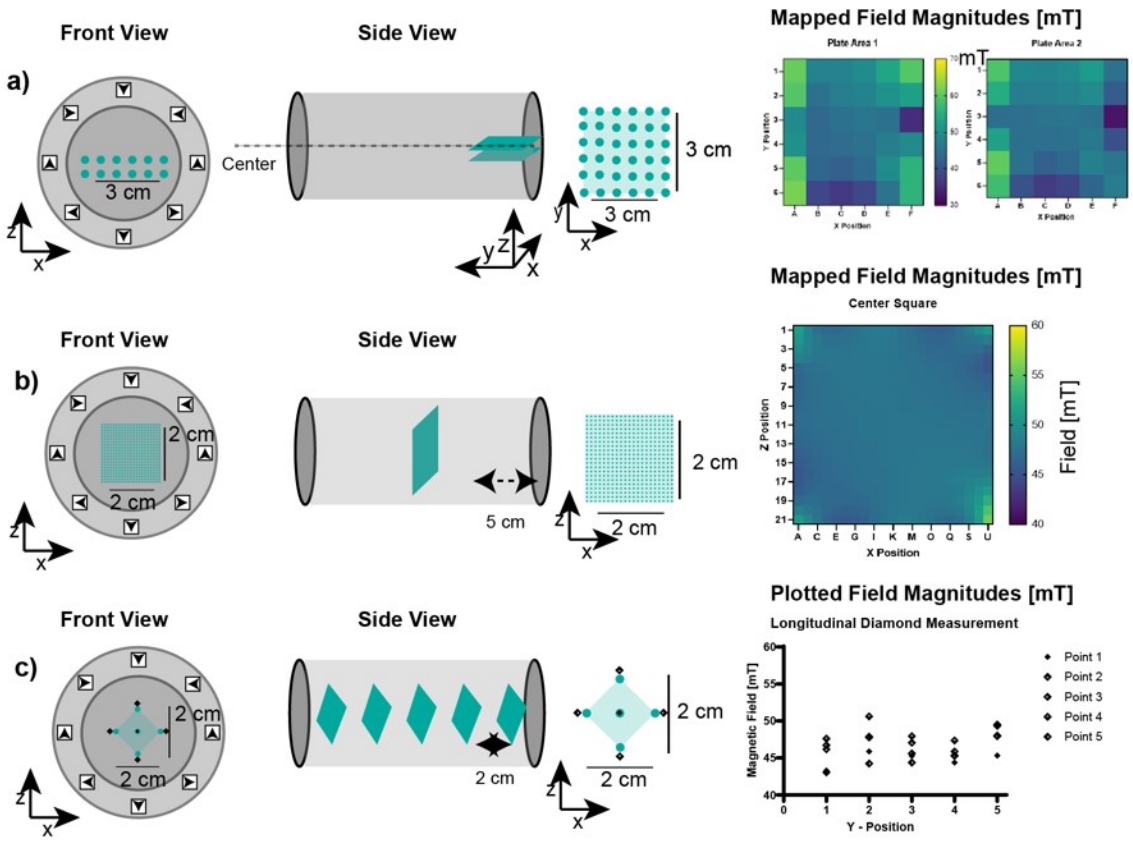

Supplementary Figure S6: Magnetic field characterization of the Halbach cylinder Different sets of measurements were collected to characterize the field magnitude within in the previously described Halbach cylinder. The left column of sketches displays the front view of the cylinder, in the center, the cylinder is depicted from the side. Blue dots indicate locations of individual measurement points. The right column of images displays color-coded maps of measured magnetic field magnitudes, displayed in mT. The analysis of the magnetic field characterization indicated a high homogeneity of the generated magnetic field. An approximate field magnitude 50 mT was achieved throughout the cylinder in center regions where the samples would be placed during experimental procedures. To incubate samples, small plastic containers containing PBS-soaked sterile tissues were placed next to the samples to avoid sample dehydration. Experiments without exposure to magnetic fields were incubated in humidified petri dishes. **a)** Two planes were mapped inside the cylinder at locations that marked the upper and lower edges of the applied cell culture ware. **b)** A square was mapped in the center of the cylinder to investigate homogeneity of the field magnitude. **c)** To investigate differences in magnetic field magnitude at positions in the center and towards the edge of the cylinder, repeated measurements were taken as indicated by the diamond-shaped array for different positions inside the Halbach cylinder.

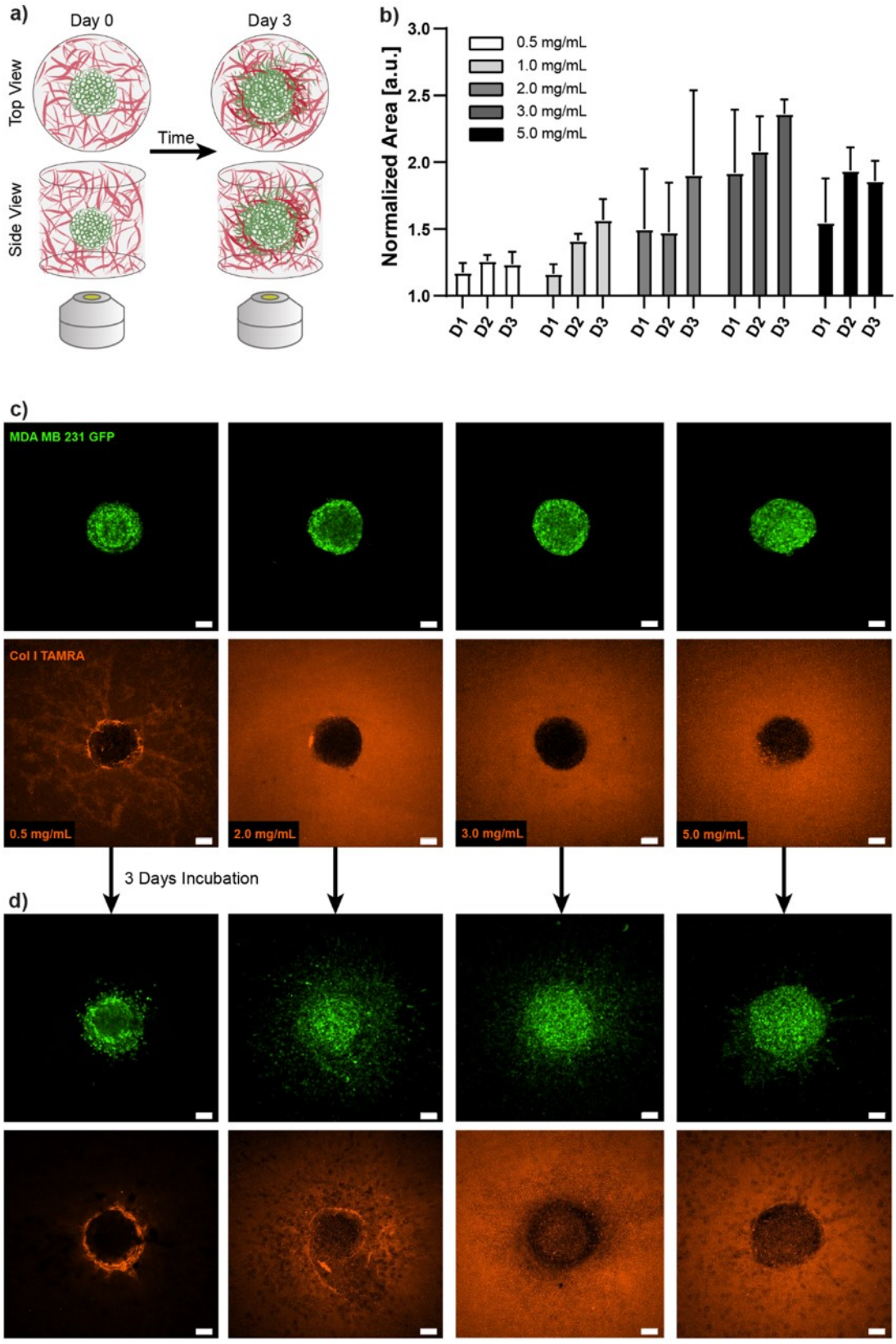

Supplementary Figure S7: Concentration-dependent invasive behavior of invasive cancer cells to the surrounding extracellular matrix

a) Tumor cell invasion is modeled by embedding of tumor spheroids from the invasive breast cancer cell line MDA MB 231 (displayed in green) in Col I hydrogel matrices (labelled in red). Tumor cell invasion is investigated by repeated imaging and analysis

of cellular spreading into the surrounding matrix network. (Indicated by the objective). **b)** Tumor cell invasion was tested for different concentrations of Col I hydrogels, between 0.5 and 5 mg/mL and analyzed for invasion of cancer cells via confocal fluorescence microscopy over three days of culture. The area of tumor cell spreading on fluorescence images was analyzed using FIJI and normalized with the area determined for images acquired 1 hour post embedding of the tumor spheroids. The graph shows mean and standard deviation. (n=4) **c)** Representative fluorescence confocal images as acquired and processed for the analysis of tumor cell invasion into the surrounding Col I hydrogel matrix. Examples for concentrations between 0.5 mg/mL and 5 mg/mL are shown. MDA MB 231 GFP cells are depicted in the top row, TAMRA-labelled Col I hydrogels are shown in red in the images of the bottom row. Data is shown for Day 0, imaged 1 hour post embedding of the tumor spheroids. **d)** Confocal fluorescence images of samples shown in c), imaged after 3 days of incubation. All scale bars: 100 µm.

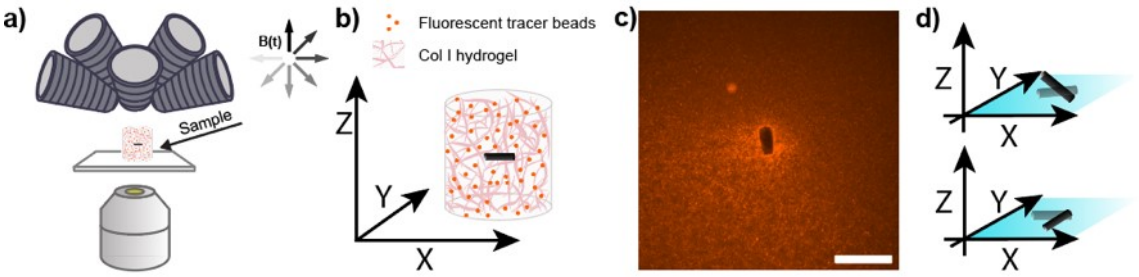

Supplementary Figure S8: Experimental setup for the analysis of Col I hydrogel deformation in response to magnetic actuation of sample-embedded magnetic µRods a) Samples were imaged during cyclic magnetic actuation using an eight-coil magnetic field generator. **b)** Fluorescent tracer beads (red) dispersed in the Col I hydrogels allowed to track Col I hydrogel deformation in response to magnetic actuation. **c)** Representative image of an iron µRod embedded in a Col I hydrogel (2 mg/mL) enriched with fluorescent microparticles (indicated in orange-red). Scale bar: 50 µm. d) Out of plane (top sketch) and in plane rotating magnetic fields (bottom sketch) were used to actuate Col I-embedded µRods to capture the 3D character of the sample volumes.

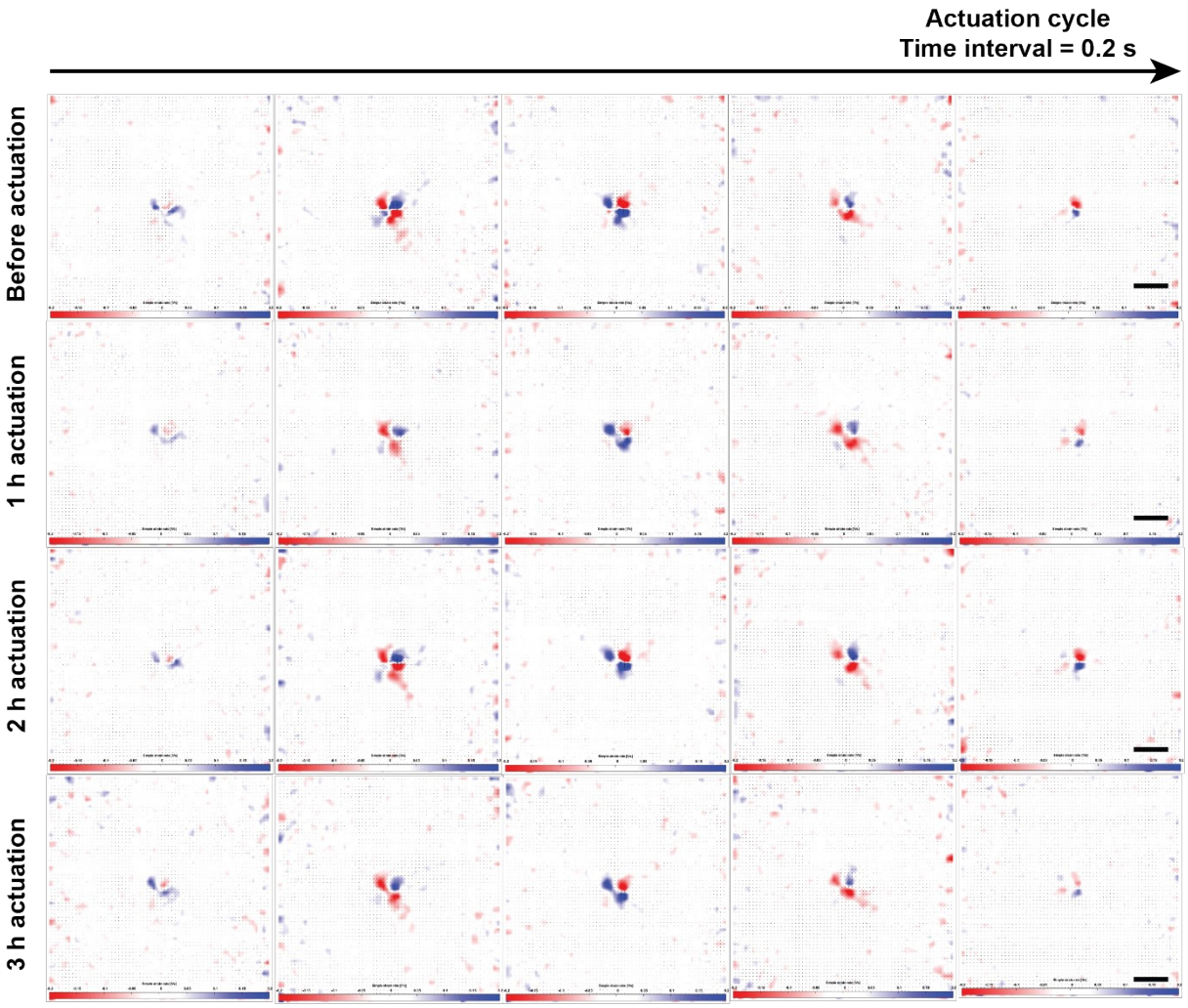

Supplementary Figure S9: Analysis of Col I hydrogel deformation upon in-plane deflection of an embedded µRod during 3 hours of magnetic actuation

Iron µRods were embedded in a Col I hydrogel (2 mg/mL) enriched with fluorescent microparticles Magnetic actuation was performed using an in-plane rotating magnetic field of 50 mT magnitude with a rotational frequency of 1 Hz. Images were acquired with a frame rate of 100 ms. Particle Image Velocimetry analysis of the image sequence was performed and then the simple strain rates were extracted at different timepoints. Scale bars: 50 µm.

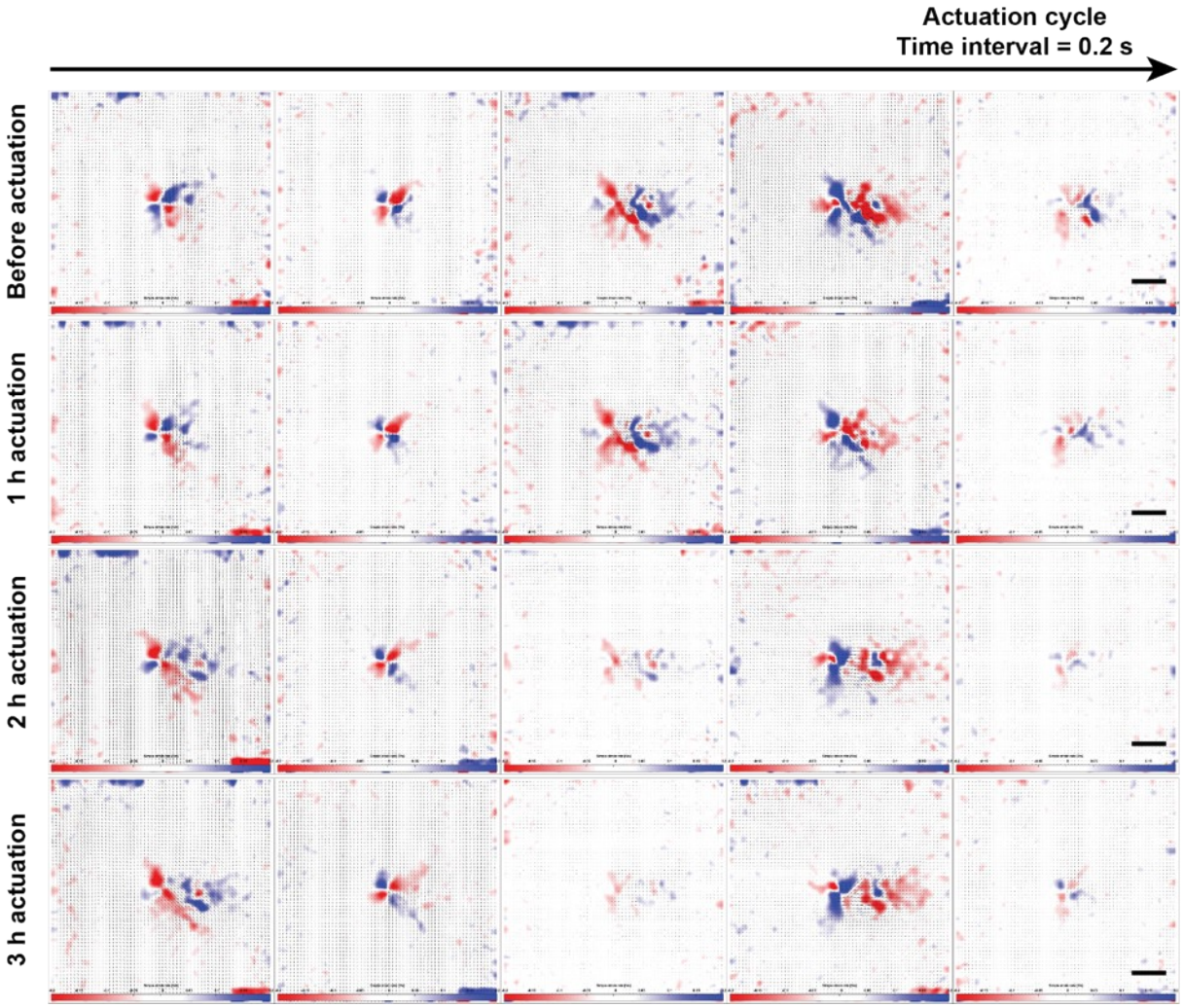

Supplementary Figure S10: Analysis of Col I hydrogel deformation upon out-of-plane deflection of an embedded µRod during 3 hours of magnetic actuation

Iron µRods were embedded in a Col I hydrogel (2 mg/mL) enriched with fluorescent microparticles Magnetic actuation was performed using an out-of-plane rotating magnetic field of 50 mT magnitude with a rotational frequency of 1 Hz. Images were acquired with a frame rate of 100 ms. Particle Image Velocimetry analysis of the image sequence were performed and then the simple strain rates were extracted at different timepoints. Scale bars: 50 µm.

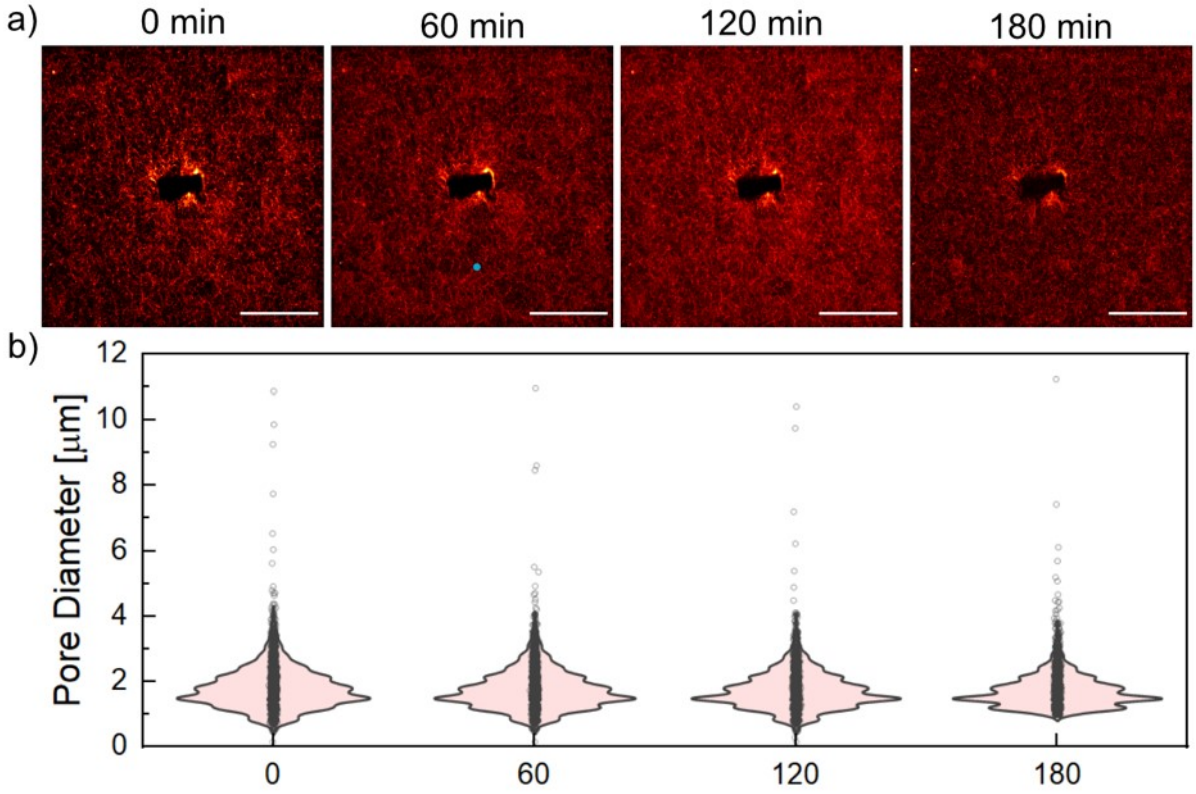

Supplementary Figure S11: Local structure of Col I hydrogel unaltered by three consecutive days of continuous actuation.

Magnetic actuation of hydrogel-embedded µRods was performed in a rotating Halbach cylinder using an out-of-plane rotating magnetic field of 50 mT magnitude with a rotational frequency of 1 Hz. **a)** Confocal fluorescence micrographs of TAMRA-labeled Col I hydrogels (2 mg/mL) over three consecutive days of continuous actuation (top row) and control samples without actuation (bottom row). Scale bar: 50 µm. **b)** Col I hydrogel (2 mg/mL) network porosity of µRod actuated and unactuated control samples.

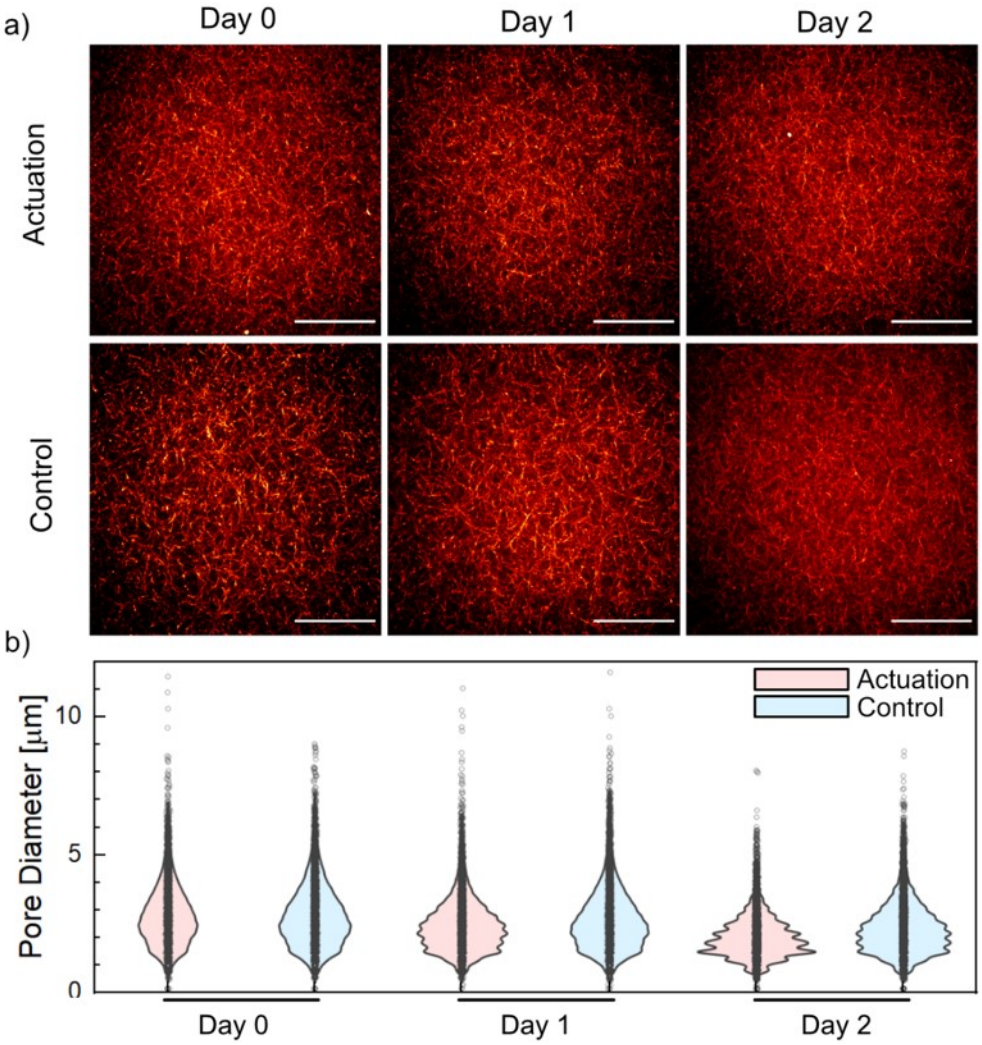

Supplementary Figure S12: Local structure of Col I hydrogel in the vicinity of a single µRod unaltered by three hours of actuation.

Magnetic actuation of hydrogel-embedded µRods was performed using an out-of-plane rotating magnetic field of 50 mT magnitude with a rotational frequency of 1 Hz. **a)** Confocal fluorescence micrographs of a TAMRA-labeled Col I hydrogel (2 mg/mL) in the vicinity of a µRod over three hours of actuation. Scale bar: 50 µm. **b)** Col I hydrogel (2 mg/mL) network porosity changes after 60, 120, and 180 minutes of actuation. The image processing pipeline to calculate the network porosity included an algorithm that determines tube-like structures (Col I fibres) based on the eigenvalues of a generated Hessian matrix, Binarization, and a Euclidean Distance Transform (EDT) which provides distance information to the closest boundaries in gray level intensities. Based on the generated EDT data the network‘s pore size was calculated.

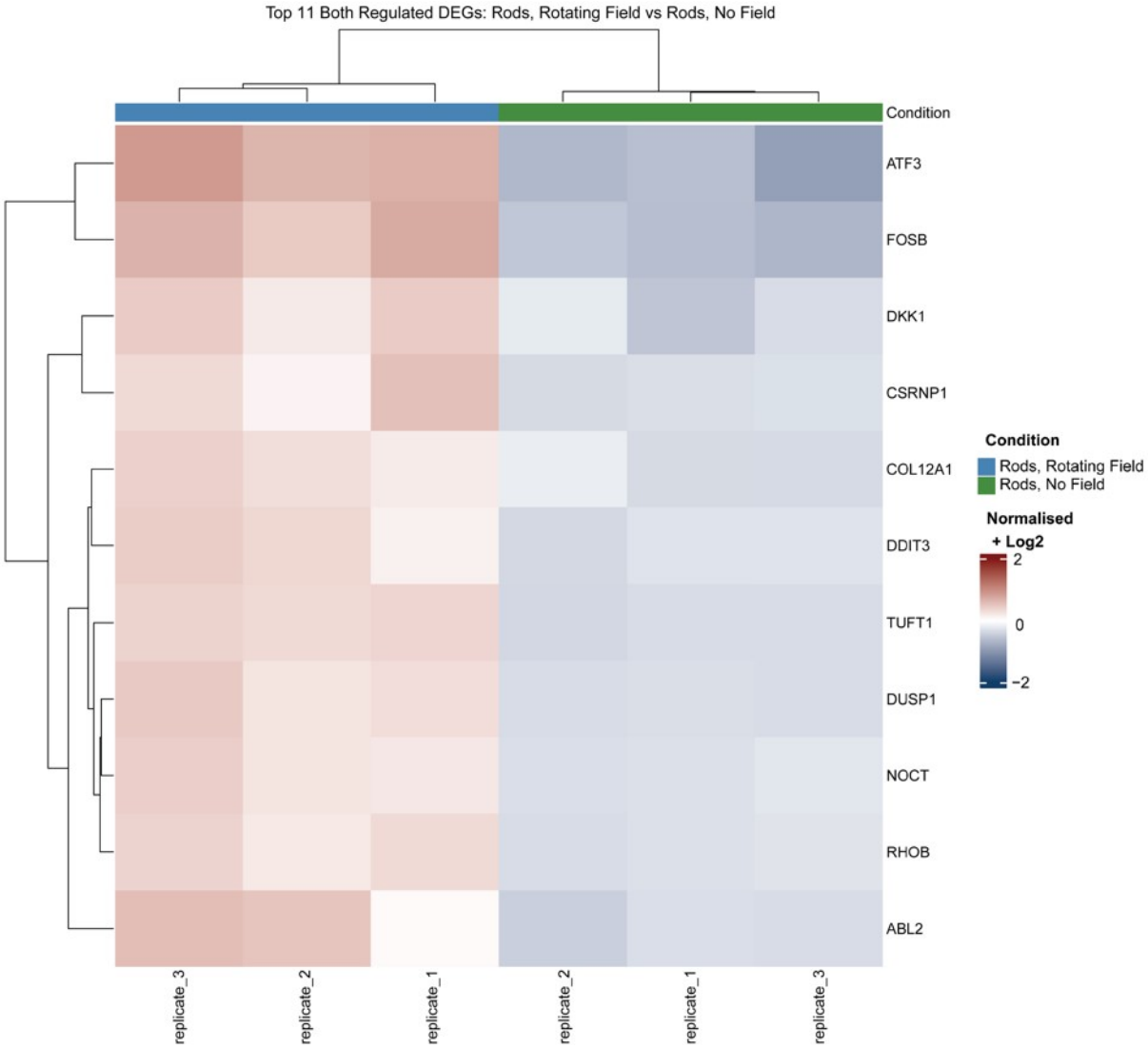

Supplementary Figure S13: RNA seq analysis of tumor spheroids with and without cyclic deformation.

Heat map based on corrected p-values (controlling the FDR at 5%) showing 11 upregulated genes for spheroid samples (n=3) exposed to cyclic deformation vs unexposed spheroids (n=3).

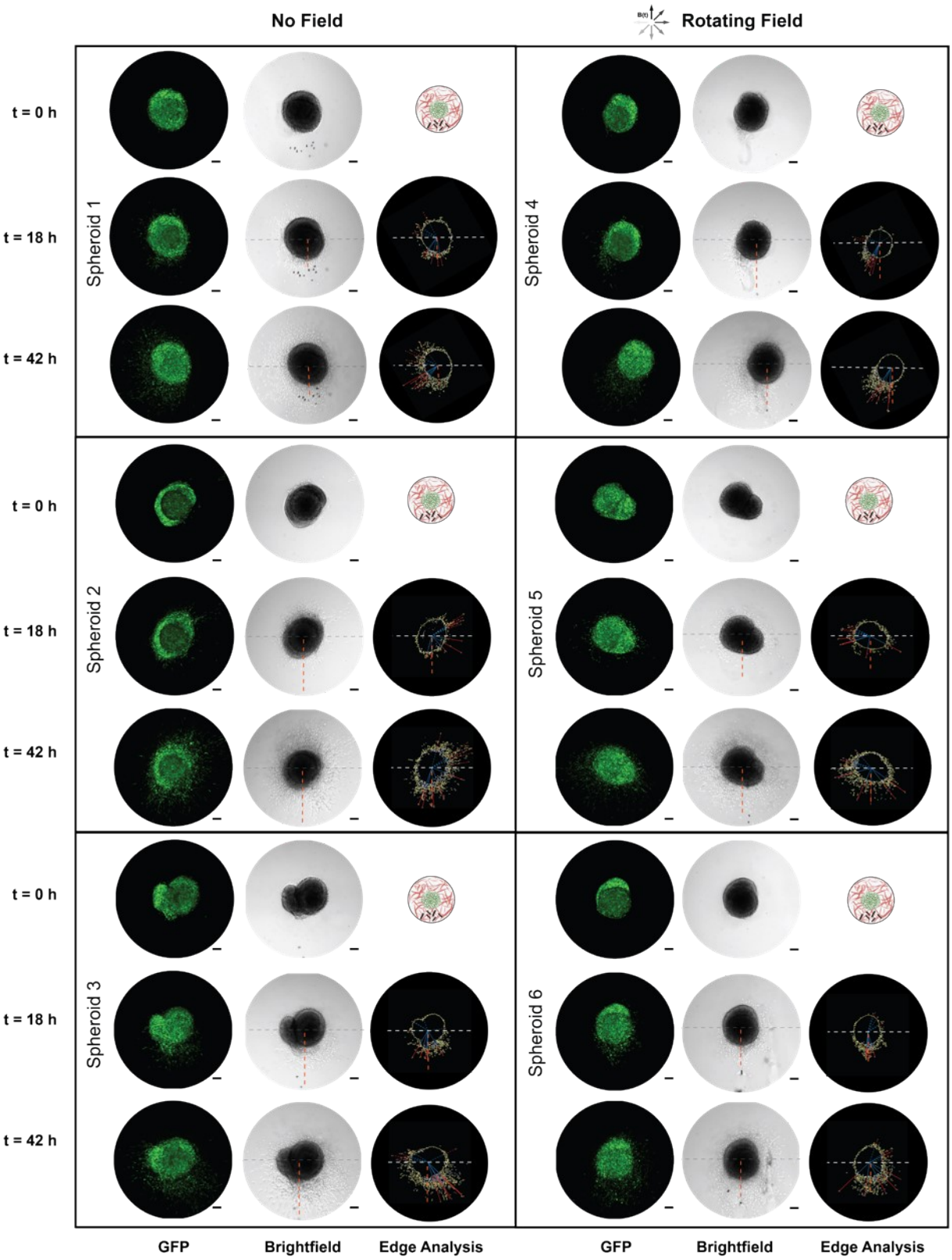

Supplementary Figure S14: Investigation of tumor cell invasion in response to local actuation

MDA-MB-231 GFP tumor spheroids embedded in Col I hydrogels at a concentration of 2 mg/mL were supplemented with a layer of Col I and functionalized iron µRods were applied as local actuators on the periphery of the tumor spheroid, then imaged after 0, 18 and 42 hours, of incubation, respectively, and after exposure to RMF of 50 mT magnitude (or no field) under standard cell culture conditions. Edge analysis was

performed for each spheroid to identify invasive cells (see Materials & Methods). Cell invasion was quantified through dividing the images into two zones (gray dashed line) – with and without μRods. The division line is derived by taking orthogonal line of relative position between μRods and the center of primary tumor (orange dashed line). In each zone, furthest five invasive cells were collected, and the invasion zone (red line) was calculated by subtracting the radius of the primary tumor (blue line) from distance of invasive cells from center of the primary tumor. All scale bars: 100 μm.

Supplementary Videos

Supplementary Video V1: Microscopy recording with a 40x objective of embedded µRod actuation (50mT, 1Hz) in Col I networks during in-plane magnetic actuation to assess strain rates

Supplementary Video V2: Microscopy recording with a 40x objective of embedded µRod actuation (50mT, 1Hz) in Col I networks during out-of-plane magnetic actuation to assess strain rates

Supplementary Video V3: Ca^{2+} influx imaging during magnetic actuation

Bibliography

1 B. Özkale Edelmann, ETH Zürich, 2016.

2 C. C. J. Alcântara, F. C. Landers, S. Kim, C. De Marco, D. Ahmed, B. J. Nelson and S. Pané, *Nat Commun*, 2020, **11**, 5957.

3 J. Kim, P. Seidler, L. S. Wan and C. Fill, *J Colloid Interface Sci*, 2009, **329**, 114–119.

4 D. O. Asgeirsson, M. G. Christiansen, T. Valentin, L. Somm, N. Mirkhani, A. H. Nami, V. Hosseini and S. Schuerle, *Lab Chip*, 2021, **21**, 3850–3862.

5 *Proceedings of the Royal Society of London. A. Mathematical and Physical Sciences*, , DOI:10.1098/rspa.1971.0044.

6 M. Sato and Y. Ishii, *J Appl Phys*,, DOI:10.1063/1.343481.